Effect of surface morphology and interfaces on longitudinal phonon thermal conductivity in Ge(001) and Si/Ge(001) thin-film structures

© A.L. Khamets [1], I.V. Safronov [2], A.B. Filonov [1], D.B. Migas [1,3,¶]

[1] Belarusian State University of Informatics and Radioelectronics,
220089 Minsk, Belarus
[2] Belarusian State University,
220030 Minsk, Belarus
[3] National Research Nuclear University „MEPhI",
115409 Moscow, Russia

[¶] E-mail: migas@bsuir.by

In this work the method of non-equilibrium molecular dynamics was used to study the longitudinal phonon thermal transport at 300 K in nanoscale homogenous Ge(001) and layered Si/Ge(001) thin films with $p(2 \times 1)$ surface reconstruction along different directions. The appearance of thermal transport anysotropy in the films under consideration, which is due to both the surface morphology and sharp Si/Ge interfaces, has been established. For the direction when the dimers and Si−Ge bonds at the interface lie in a plane parallel to the direction of the heat flow, the lowest thermal conductivity is observed ($\sim 5-18$ W/(m · K) in the range from ~ 1 to 27 nm). It is shown that for films with thicknesses of more than 13 nm for all directions, layered films have a lower thermal conductivity compared to homogenous ones. In this case, the role of the surface morphology and interfaces is reduced to different degrees of phonon localization and compensation for more heat-conducting Si layers, respectively.

Keywords: thermal conductivity, molecular dynamics, Si/Ge thin-film, surface, interfaces.

1. Introduction

The main disadvantage of the known thermoelectric materials is their low efficiency of conversion of thermal energy into electrical energy [1]. The efficiency of thermoelectric energy conversion can be estimated using the dimensionless thermoelectric figure of merit $ZT = S^2 \sigma T / (\kappa_L + \kappa_e)$, where S is the Seebeck coefficient, σ is the electrical conductivity of the material, κ_L, κ_e are the phonon (lattice) and electronic components of the thermal conductivity, T is the working temperature. One of the key approaches to increasing the thermoelectric figure of merit of semiconductor materials is to reduce their phonon thermal conductivity [2]. Low-dimension materials based on Si and Ge, such as thin films, nanowires, have been of great interest to researchers in the last few decades due to the increased effective scattering of phonons at interfaces and surfaces [3]. A significant decrease in thermal conductivity in comparison with bulk Si and Ge (the thermal conductivity of which is 140 [4] and 55 W/(m · K) [5], respectively) in similar nanostructures (up to 0.33 W/(m · K) for a layered Au/Si film with a total thickness of 87 nm [6]) can significantly increase their thermoelectric figure of merit ZT.

In a number of papers, in particular, the anisotropy of phonon thermal conductivity in homogeneous Si [7–9], Ge [10–12], as well as in layered Si/Ge films [12,13] and bulk superlattices [12–16] has been studied. Among the listed papers, various orientations of the surface and (or) interfaces in films were considered only in [7–9,12,13]. Thus, in (001), (110), (111) and (112) oriented thin Si films, the (112)/[111] direction is characterized by the highest thermal resistance [7] or the lowest longitudinal thermal conductivity [9]. Among the three main surface orientations (001) ([100] direction), (110) ([100] and [0$\bar{1}$1]directions) and (111) ([110] and [112] directions) the lowest longitudinal thermal conductivity was found for thin Si membranes in the (001)/[100] direction [8]. The study of longitudinal phonon thermal conductivity in thin-film structures based on Si and Ge with (001), (110), and (111) orientations along one [$\bar{1}$10] crystallographic direction revealed that homogeneous Ge(001) and layered Si/Ge(001) films have the lowest values of thermal conductivity [13]. In the paper [12] for similar thin-film structures, we additionally considered other directions, however, the (001)/[$\bar{1}$10] variants with a total thickness of up to 10 nm showed the lowest longitudinal thermal conductivity.

For thin diamond films with the (001) orientation, the presence of a significant anisotropy of longitudinal thermal conductivity along the equivalent directions⟨110⟩ (i.e. [110] and [$\bar{1}$10]) was shown [17]. In particular, for a typical $p(2 \times 1)$ reconstruction of a C(001) film with a thickness of 2.1 nm, the anisotropy factor was 1.8, i.e., the thermal conductivity in the case of the heat flow
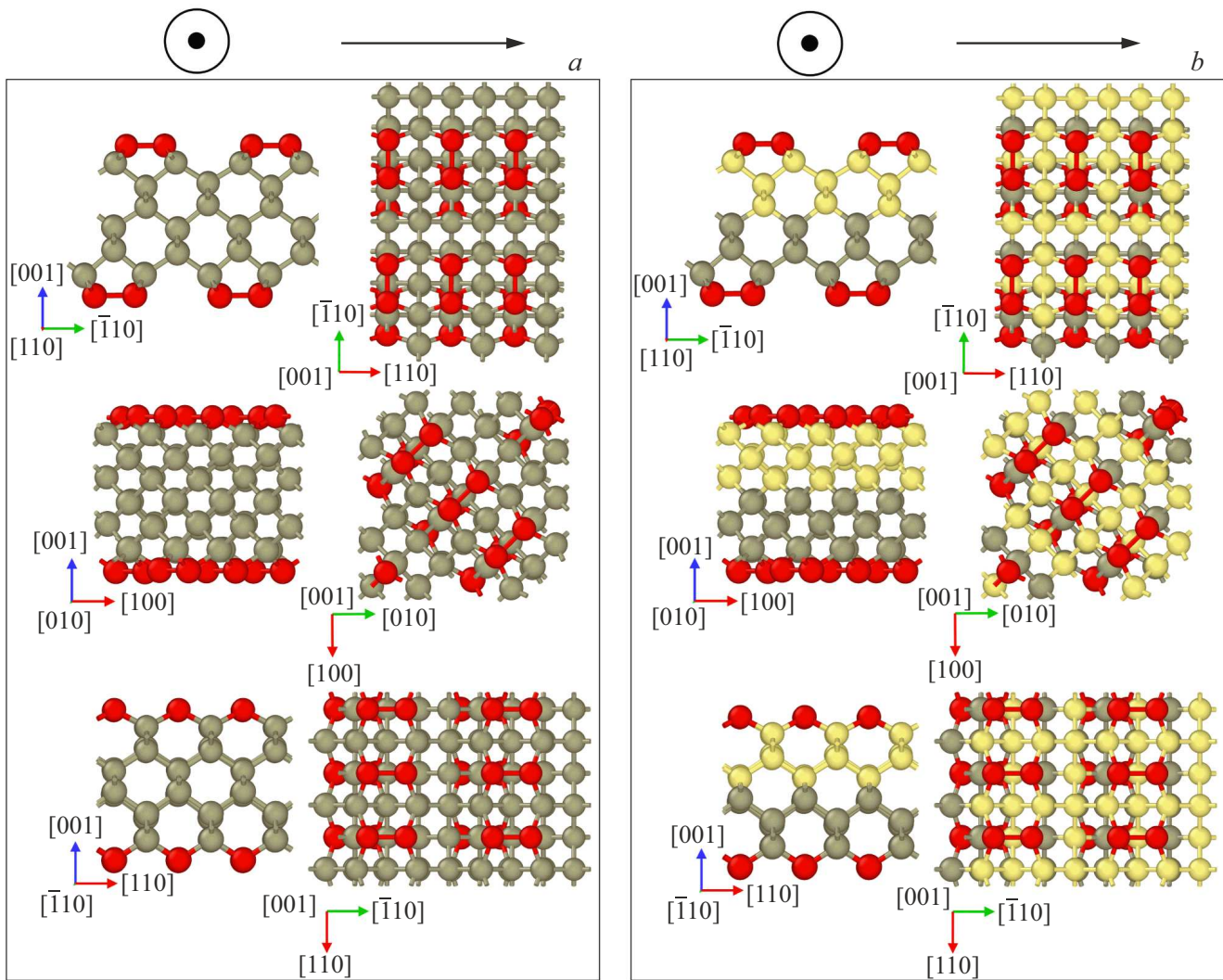
Figure 1. Models of structures of Ge(001) (*a*) and Si/Ge(001) (*b*) films with $p(2 \times 1)$ surface reconstruction in two projections along [110], [010] and [$\bar{1}$10] directions. Directions of heat flow propagation are indicated on the pictograms. Dimers are highlighted in red. (A color version of the figure is provided in the online version of the paper).

across the dimer direction is almost 2 times higher, than along dimers [17]. For thin Si and Ge films, as well as for layered Si/Ge films, similar studies have not been carried out. Thus, the purpose of this work is to study the effect of surface morphology and interfaces on the longitudinal phonon thermal conductivity in homogeneous Ge(001) and layered Si/Ge(001) films with $p(2 \times 1)$ surface reconstruction.

2. Materials and methods

In this paper, we consider (001) oriented homogeneous Ge and also layered Si/Ge films in the form of symmetric periodic superlattices with sharp interfaces (coherent phase conjugation without taking into account interdiffusion). All films were subjected to $p(2 \times 1)$ surface reconstruction by forming rows of Si−Si and (or) Ge−Ge

dimers. For a layered Si/Ge film, the Si and Ge layers had a thickness of 4 monoatomic layers (or equal to one lattice parameter: for Si is 0.543 nm, and for Ge is 0.566 nm). Together, these layers form a Si/Ge bilayer with a period of 1.1 nm, the number of which varied from $n = 1$ to 24, and this is equivalent to a thickness from 1.1 to ~ 27 nm. The choice of such a period is associated with the lowest achievable longitudinal thermal conductivity [12]. The programs Jmol [18] and OVITO [19] were used to visualize and generate these structures.

The Tersoff potential [20] was used to describe the interatomic interaction. Three-dimensional periodic boundary conditions with a vacuum gap ~ 5 nm were used for all the structures. All the structures were preliminarily optimized by the molecular statics method using the LAMMPS [21] software package. The non-equilibrium molecular dynamics method (LAMMPS [21] package)
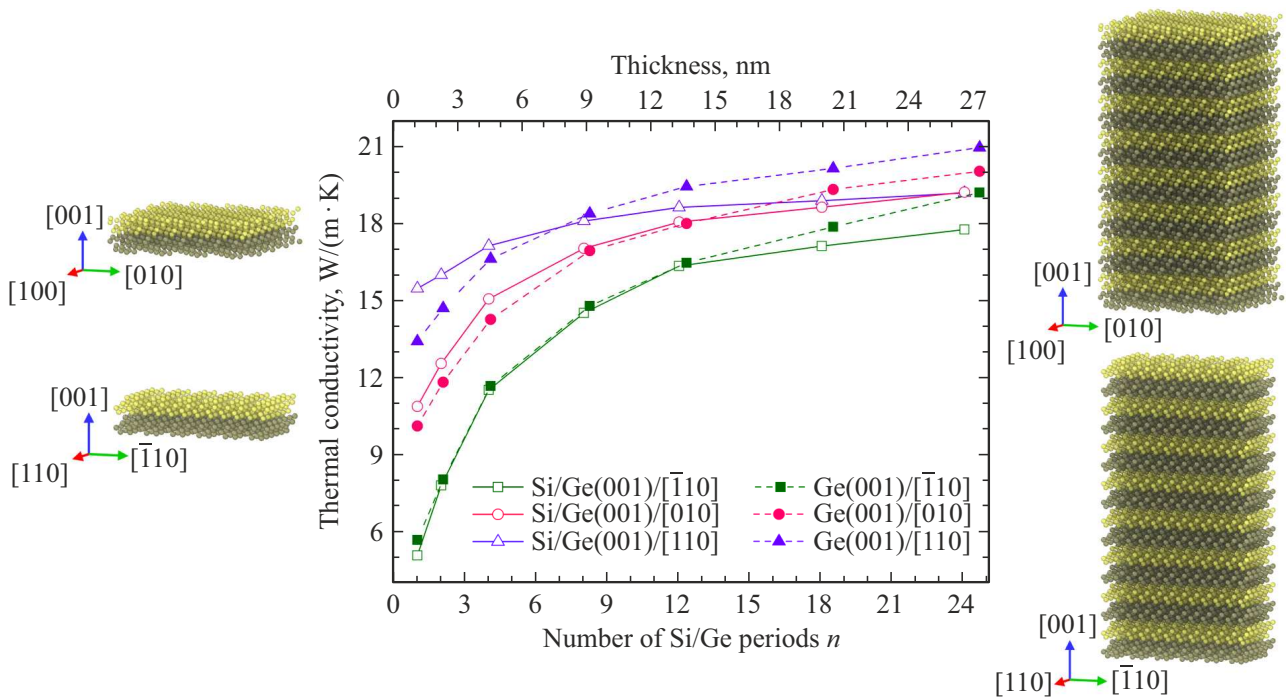
Figure 2. Longitudinal phonon thermal conductivity at 300 K of homogeneous Ge- and layered Si/Ge-films with orientation (001) on the number of periods (or total film thickness along the upper axis) along different crystallographic directions. Models of layered structures at different n are shown in the inserts.

was used to determine the phonon thermal conductivity. The structures were brought to the thermodynamically equilibrium state at $T = 300$ K using the isobaric-isothermal and canonical ensembles for 0.9 and 0.1 ns, respectively, and also with the microcanonical ensemble for 2 ns. To create a temperature gradient, Langevin thermostats (cold and hot at 290 and 310 K, respectively) were placed at a distance of half the supercell length. To neutralize the temperature fluctuations, the number of atoms in both thermostats was the same and equal to ~ 6000 atoms. The value of the phonon thermal conductivity was determined from the Fourier law after 2 ns:

$$\kappa_L = -\frac{E}{2S_{\text{sec}}\,t(dT/dx)},$$

where E is the transferred thermal energy; 2 is the factor related to heat flow in two directions; t is the simulation time; S_{sec} is the cross-section area; dT/dx is the temperature gradient in the selected crystallographic direction.

When modeling the longitudinal phonon thermal conductivity, all the structures under consideration had approximately the same supercell size (slightly over 100 nm), in order to achieve a linear response mode between the reciprocals of the thermal conductivity and the supercell size [22]. The dispersion curves, phonon group velocities, and projection vibrational densities of states (normalized) were calculated using the phonoLAMMPS [23] and Phonopy [24] programs. The Dynaphopy [25] program was used to determine the force constants at 300 K.

3. Results and discussion

Since the Tersoff potential does not take into account the electron density redistribution, it is unable to reproduce the standard, experimentally observed $p(2 \times 2)$ or $c(4 \times 2)$ reconstructions of Si(001) and Ge(001) surfaces with dimers inclined to the surface plane [26]. In our case, all dimers are parallel to the surface, thus, the $p(2 \times 1)$ surface reconstruction was initially used, on which three main low-index directions $[\bar{1}10]$, $[010]$ and $[110]$ can be distinguished (see Fig. 1). Obviously, the directions $[\bar{1}10]$ and $[110]$ are indeed non-equivalent due to the formation of dimer rows. A similar conclusion is also typical for sharp Si/Ge interfaces, for which Si−Ge bonds are directed along $[\bar{1}10]$ (Fig. 1, *b*), and this can also lead to the appearance of thermal conductivity anisotropy.

Based on the calculation results, it was found (Fig. 2) that the longitudinal thermal conductivity for both homogeneous Ge and layered Si/Ge films is minimal and maximal along the directions $[\bar{1}10]$ and $[110]$, respectively, indicating the presence of anisotropy. The highest anisotropy factor $(\gamma = \kappa_L^{[110]}/\kappa_L^{[\bar{1}10]})$ is 3.1 and 2.3 for layered Si/Ge and homogeneous Ge films at thicknesses ~ 1 nm, respectively. With an increase in the thickness of both type films up to ~ 27 nm γ decreases to 1.1. Meanwhile, the lowest values of thermal conductivity along $[\bar{1}10]$ are equal to 5.72 and 5.12 W/(m · K) for homogeneous Ge- and layered Si/Ge-films at a thickness of ~ 1 nm, respectively, and with
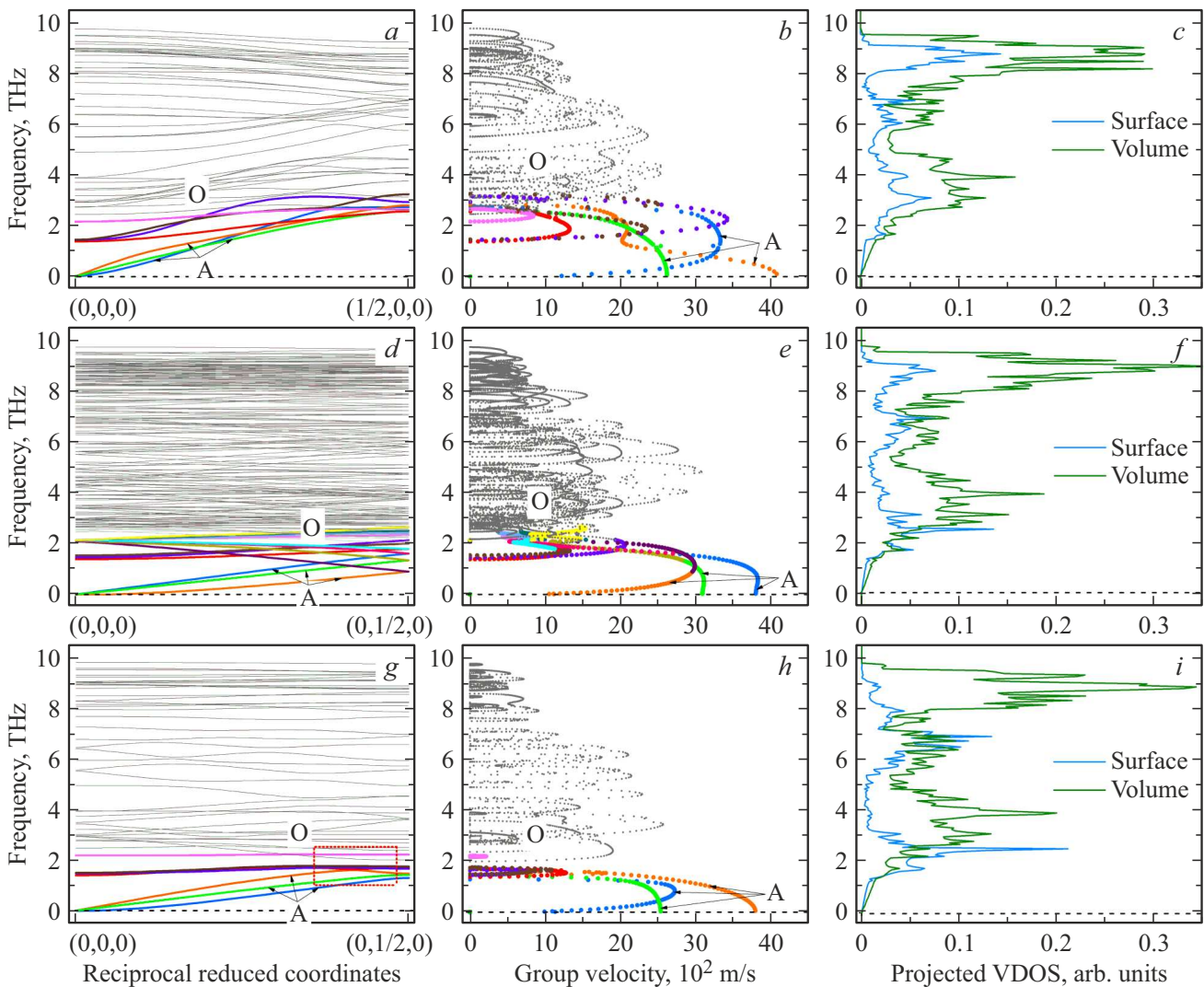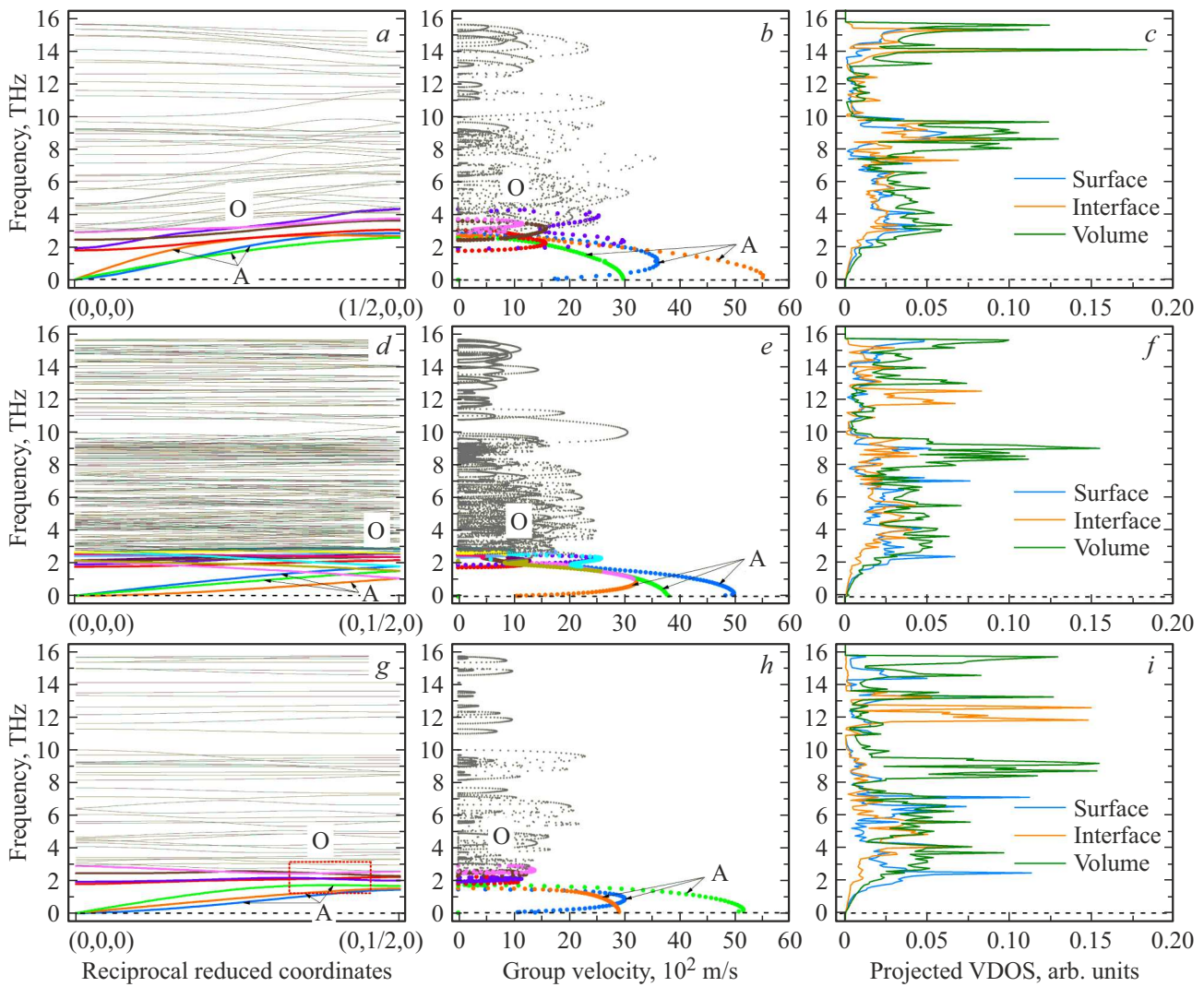
Figure 3. Dispersion curves (*a*), (*d*), (*g*), group velocities (*b*), (*e*), (*h*) and partial vibrational densities of states (*c*), (*f*), (*i*) of phonons for the case of a homogeneous Ge film with a thickness of 1.1 nm at 300 K. Acoustic (A) and optical (O) modes are marked. Direction [110] matches the figures (*a*)−(*c*), [010] — (*d*)−(*f*) and [$\bar{1}$10] — (*g*)−(*i*).

an increase in thickness, they nonlinearly reach saturation of slightly more than $18 \, W/(m \cdot K)$, which was shown in more detail previously [13]. It was also found that, exceptionally for the [$\bar{1}$10] direction, the longitudinal thermal conductivity for layered Si/Ge- and homogeneous Ge-films are comparable in the thickness range up to ~ 9 nm, in contrast to the [010] and [110] directions (Fig. 2). Meanwhile, for all crystallographic directions at a film thickness of > 13 nm, layered Si/Ge films have a lower phonon thermal conductivity compared to homogeneous Ge films, which may be due to the effective phonon scattering at interfaces. The difference in thermal conductivity between homogeneous Ge and layered Si/Ge films for the [110], [010] and [$\bar{1}$10] directions is ~ 4, 9 and 8%, respectively for the films with a thickness of ~ 27 nm.

Obviously, such a high degree of thermal conductivity anisotropy is due to the different morphology of the surface and interfaces with respect to the direction of heat flow propagation. Meanwhile, the enhancement of anisotropy in layered Si/Ge films compared to homogeneous Ge films (Fig. 2) is due to interfaces, which either compensate or do not compensate for the contribution of more heat-conducting Si layers [12,13]. The decrease in the anisotropy factor with an increase in the thickness of the films under consideration can be associated with a decrease in the role of the surface, which is gradually leveled [8,12,13,27]. As shown in [12,13], at (001) orientation, the surface plays a primary role in layered Si/Ge films with a total thickness of up to ~ 10 nm, while as the thickness increases, the main scattering mechanism changes from phonon-surface to phonon-interface. The latter is reflected in the dependences shown in Fig. 2 in the form of a divergence of curves for homogeneous and layered films (at thicknesses of > 13 nm or the number of periods more than 12), where

Figure 4. Dispersion curves (*a*), (*d*), (*g*), group velocities (*b*), (*e*), (*h*) and partial vibrational densities of states (*c*), (*f*), (*i*) of phonons for the case of a layered Si/Ge film with a total thickness of 1.1 nm (or $n = 1$) at 300 K. Acoustic (A) and optical (O) modes are marked. Direction [110] matches the figures (*a*)−(*c*), [010] — (*d*)−(*f*) and [$\bar{1}$10] — (*g*)−(*i*).

for the former, there is a further increase in thermal conductivity, while for the latter, this growth is already slowing down.

For a correct interpretation of the results obtained, an analysis of dispersion curves, frequency dependences of group velocities, and partial vibrational densities of states of phonons for homogeneous Ge (Fig. 3) and layered Si/Ge (Fig. 4) films with the smallest thicknesses is also given. As can be seen from Fig. 3, *a* — 4, *a*, 3, *d* — 4, *d* and 3, *g* — 4, *g*, for both types of films, the acoustic branches reach higher values in frequency for the [110] direction compared to the [010] and [$\bar{1}$10] directions. It should be noted that for the case of [$\bar{1}$10], there is a strong acoustic-optical coupling (highlighted by dotted frames in Figs 3 and 4), leading to strong resonant scattering [28,29]. As a consequence, the highest and lowest group velocities of phonons are characteristic of the [110] (Fig. 3, *b* — 4, *b*) and [$\bar{1}$10] (Fig. 3, *h* — 4, *h*) directions,

respectively, which leads to the observed difference in thermal conductivity (Fig. 2).

The normalized vibrational densities of states shown in Fig. 3, *c* — 4, *c*, 3, *f* — 4, *f*, 3, *i* — 4, *i*, demonstrate a significant contribution of surface modes to the total density of states compared to bulk modes. It is for the [$\bar{1}$10] direction that the greatest discrepancy between the phonon spectra of surface and bulk atoms is observed, which consists in the peak shift for surface atoms towards lower frequencies (Fig. 3, *i* — 4, *i*). In particular, the increased values of the density of states in the vicinity of 2.5 THz (Fig. 3, *i* — 4, *i*) indicate the phonon surface localization [30], which results in a decrease in the thermal conductivity of such homogeneous Ge- and layered Si/Ge-films.

The phonon spectra of interface and surface atoms are comparable in a layered Si/Ge film only for the [110] direction (Fig. 4, *c*). The smallest and largest mismatches

between the phonon spectra of interface and bulk atoms are characteristic of the $[110]$ and $[\bar{1}10]$ directions, respectively (Fig. 4, c and i). In case of the $[\bar{1}10]$ direction, there is a significant suppression of the peaks over the entire frequency range, as well as „cutting" of the spectrum from the high-frequency side ($\sim 14-16$ THz) with a shift of the peaks towards low frequencies by ~ 2 THz, which can also be a consequence of more efficient phonon-interface scattering [31]. Thus, there is the most efficient phonon-interface scattering when the Si−Ge bonds at the interface lie in a plane parallel to the direction of heat flow propagation. Let us note that in the first case ($[\bar{1}10]$) the interfaces compensate, while in the second case ($[110]$) they do not compensate (in the range up to ~ 9 nm) the contribution of more heat-conducting Si layers, which agrees with data in Fig. 2 when comparing the thermal conductivity of homogeneous and heterogeneous films.

In contrast to [17], where the anisotropy of longitudinal thermal conductivity was found in nanosized C(001) films along the $[110]$ and $[\bar{1}10]$ directions, this effect was detected not only for homogeneous Ge(001), but also for layered Si/Ge(001) films. The anisotropy factors for Ge(001) and C(001) films of equivalent thicknesses (~ 2 nm) coincide ($\gamma \cong 1.8$), however, with the same number of atomic layers (24) γ for a germanium film is already lower compared to a diamond one ($\gamma \sim 1.6$) due to the larger lattice parameter. At the same time, for Si/Ge(001) films of equivalent thickness, the anisotropy factor is higher ($\gamma \cong 2.1$), which emphasizes, along with the surface, the role of interfaces in the occurrence of anisotropy.

4. Conclusion

Using the method of non-equilibrium molecular dynamics, the effect of surface morphology and interfaces on the longitudinal phonon thermal conductivity along the $[110]$, $[010]$ and $[\bar{1}10]$ directions at 300 K was studied for (001) oriented homogeneous Ge- and layered Si/Ge-films with a thickness from 1.1 to ~ 27 nm with $p(2 \times 1)$ surface reconstruction. Due to the lower group velocities of phonons and the presence of strong acoustic-optical coupling, the $[\bar{1}10]$ direction, in which the dimers are located along the direction of the heat flow, demonstrates the lowest thermal conductivity values for both homogeneous Ge- ($\sim 6-19$ W/(m · K)) and layered Si/Ge films ($\sim 5-18$ W/(m · K)) over the entire range of film thicknesses. In addition, in the case of the $[\bar{1}10]$ direction in layered Si/Ge films, when the Si−Ge bonds at the interface lie in a plane parallel to the heat flow, the contribution of more heat-conducting Si layers is compensated due to the effective scattering of phonons by sharp interfaces. The maximum values of thermal conductivity are characteristic for the ($\sim 16-19$ W/(m · K) in the thickness range $\sim 1-27$ nm) case of heat flow propagation in the direction perpendicular to the plane with dimers and Si−Ge bonds at the interface. With an increase in the total thickness of the layered films above ~ 13 nm

(the number of periods is more than 12), a change in the main scattering mechanism from the phonon-surface to the phonon-interface was found.

From the results obtained, it can also be concluded that, in the case of other surface reconstructions and orientations in thin films based on Si and Ge, a similar effect associated with the manifestation of strong anisotropy for thermal transport is possible to be observed. For a more reliable assessment of the effectiveness of such materials for thermoelectric applications, it is necessary to further evaluate the effect of structural defects, as well as oxidation of free surfaces, on phonon thermal conductivity.

Conflict of interest

The authors declare that they have no conflict of interest.

References

[1] Z.-G. Shen, L.-L. Tian, X. Liu. Energy Convers. Management, **195**, 1138 (2019).

[2] G.J. Snyder, E.S. Toberer. Complex Thermoelectric Materials, **7**, 105 (2008).

[3] J.A. Pérez-Taborda, O. Caballero-Calero, M. Martín-González. *New Research on Silicon — Structure, Properties, Technology* (InTechOpen, London, 2017).

[4] H.R. Shanks, P.D. Maycock, P.H. Sidles, G.C. Danielson. Phys. Rev., **130** (5), 1743 (1963).

[5] A.F. Ioffe. Canadian J. Phys., **34** (12A), 1342 (1956).

[6] E. Dechaumphai, D. Lu, J.J. Kan, J. Moon, E.E. Fullerton, Z. Liu, R. Chen. Nano Lett., **14** (5), 2448 (2014).

[7] P. Heino. Eur. Phys. J. B, **60**, 171 (2007).

[8] Z. Aksamija, I. Knezevic. Phys. Rev. B, **82** (4), 045319 (2010).

[9] H. Karamitaheri, N. Neophytou, H. Kosina. J. Appl. Phys., **113**, 204305 (2013).

[10] Z.H. Wang, M.J. Ni. Heat Mass Transfer, **47** (4), 449 (2011).

[11] X. Zhang, X. Wu. Comput. Mater. Sci., **123**, 40 (2016).

[12] A.L. Khamets, I.I. Khaliava, I.V. Safronov, A.B. Filonov, D.B. Migas. Japan. J. Appl. Phys., **62**, SD0804 (2023).

[13] A.L. Khomets, I.I. Kholyavo, I.V. Safronov, A.B. Filonov, D.B. Migas. Fiz. Tverd. Tela, **64** (5), 564 (2022) (in Russian).

[14] J. Garg, G. Chen. Phys. Rev. B, **87** (14), 140302 (2013).

[15] Z. Aksamija, I. Knezevic. Phys. Rev. B, **88** (15), 155318 (2013).

[16] A. Kandemir, A. Ozden, T. Cagin, C. Sevik. Sci. Technol. Adv. Mater., **18** (1), 187 (2017).

[17] X. Liu, G. Zhang, Y.-W. Zhang. Carbon, **94**, 760 (2015).

[18] Jmol: an open-source Java viewer for chemical structures in 3D: http://www.jmol.org/

[19] A. Stukowski. Modelling Simul. Mater. Sci. Eng., **18**, 015012 (2009).

[20] J. Tersoff. Phys. Rev. B, **39** (8), 5566 (1989).

[21] S. Plimpton. J. Comput. Phys., **117**, 1 (1995).

[22] Y. He, I. Savić, D. Donadio, G. Galli. Phys. Chem. Chem. Phys., **14** (47), 16209 (2012).

[23] A. Carreras. (2021), phonoLAMMPS: A python interface for LAMMPS phonon calculations using phonopy (0.8.1), Zenodo (https://doi.org/10.5281/zenodo.5668319)

[24] A. Togo, I. Tanaka. Scr. Mater., **108**, 1 (2015).

[25] A. Carreras, A. Togo, I. Tanaka. Comput. Phys. Commun., **221**, 221 (2017).

[26] D.B. Migas, P. Raiteri. L. Miglio, A. Rastelli, H. von Känel. Phys. Rev. B, **69**, 235318 (2004).

[27] X. Wang, B. Huang. Sci. Rep., **4**, 6399 (2014).

[28] H. Zhu, C. Zhao, P. Nan, X-m. Jiang, J. Zhao, B. Ge, C. Hiao, Y. Xie. Chem. Mater., **33**, 1140 (2021).

[29] H. Xie. Mater. Lab., **1**, 220051 (2022).

[30] F. Sansoz. Nano Lett., **11**, 5378 (2011)

[31] M. Hu, K.P. Giapis, J.V. Goicochea, X. Zhang, D. Poulikakos. Nano Lett., **11**, 618 (2011).

Translated by E. Potapova